SRR Based Compact Wideband Metamaterial Inspired Antenna for WiMAX (2.5–2.7)/WLAN (2.4–2.48)/Bluetooth (2.4–2.48)/LTE (2.3–2.4) Applications

Manish Sharma, Naveen Mishra, and Raghvendra Kumar Chaudhary[*]

Abstract—An SRR based compact wideband metamaterial inspired antenna for WiMAX (2.5–2.7)/WLAN (2.4–2.48)/Bluetooth (2.4–2.48)/LTE (2.3–2.4) applications has been fabricated and investigated in this paper. The proposed antenna structure has been designed with the concept of epsilon negative transmission line. It comprises a patch on the top of the substrate and SRR and ground connected through strip on the bottom of the substrate. The proposed antenna offers overall electrical dimensions of $0.29\lambda_0 \times 0.19\lambda_0 \times 0.015\lambda_0$ where λ_0 represents the free space wavelength at the frequency of 2.88 GHz. Additionally, the designed antenna also provides simulated and measured -10 dB fractional bandwidths of 40.13% and 40.55% around the center frequencies of 2.89 and 2.88 GHz, respectively. The average simulated and measured total gains of the proposed antenna throughout the working band are 1.92 dB and 1.75 dB. Further the average simulated radiation efficiency throughout the entire -10 dB bandwidth of the deigned antenna is 96.2%.

1. INTRODUCTION

In the last decade, the extensive demand for compact electronic gadgets of wireless communication has been increased. Metamaterial [1] rises as the best suited alternative to fulfill the demand for compact antennas. Metamaterial structures grab the attention of researchers, due to its unconventional properties such as anti-parallel group velocity and phase velocity [2, 3]. Designing of these compact antennas was a challenging task for the researchers, as it suffers from a lot of problems. Some of them can be listed as poor radiation efficiency [4, 5] and narrow bandwidth [6–8]. Numerous approaches have been scrutinized to design a compact antenna. For this purpose, dielectric loading is a facile way in which a high dielectric constant substrate is used [8].

Apart from antennas, the characteristics of metamaterial structures are also utilized for designing filters [9, 10] and ultra-thin absorbers [11, 12]. Gupta et al. [7] discusse a compact dual-band metamaterial antenna. This antenna is designed with an interdigital capacitor and a rectangle-shaped complementary split ring resonator. Rectangular split ring resonator has been utilized to offer compactness to the antenna by introducing one resonance peak at the lower frequency band. In [13], a complementary split ring resonator is used to design a wideband antenna. In this configuration, one unit cell of composite right/left transmission line is introduced into a patch antenna. In this regards, a inter digital capacitor in the patch and split ring resonator at the bottom ground plane are created. Although this article claims about antenna electrical size of $0.24\lambda_0 \times 0.24\lambda_0$, the overall size of the antenna is $0.50\lambda_0 \times 0.44\lambda_0$. In the last decade, several articles have been reported and claim about wideband property by optimizing the series and shunt parameters of the antennas [2, 14, 15]. In [2, 14],

short ended boundary condition has been applied which confirms that in these antennas zeroth order resonance (ZOR) frequency and bandwidth can be controlled with the series parameter of unit cell. In a similar fashion, [15] applies open ended boundary condition and controls the ZOR frequency and bandwidth with the variation of shunt parameters. Another approach utilized to improve the bandwidth of the compact metamaterial antennas is mode merging [16]. In [16], two transmission line metamaterial arms have been used to achieve dual resonances which are further merged to improve the bandwidth of antenna structure. In the year of 2015, Kenari et al. introduced a composite right/left-handed transmission line based metamaterial antenna designed with slots and spiral inductor and can operate in 5.8 to 7.3 GHz band [17]. Further, metamaterial based leak wave and travelling wave antennas are discussed in [18, 19].

This article presents an SRR based compact wideband metamaterial inspired antenna, which can be used for several applications such as WiMAX, WLAN, Bluetooth and LTE. In order to improve the working bandwidth of the designed antenna, SRR is configured with the designed antenna. The design approach for the proposed antenna utilizes the concept of epsilon negative transmission line.

2. ANTENNA DESIGN AND ANALYSIS

The proposed antenna structure is designed on a two sided copper coated FR-4 epoxy glass substrate (dielectric constant of 4.4, loss tangent $= 0.02$, and thickness $= 1.6$ mm). Top of the substrateis configured with a feed-line and rectangular patch while SRR along with a thin stripline which connects SRR to ground plane is printed on the bottom of the substrate as shown in Figs. 1(a) and 1(b), respectively.

An equivalent circuit diagram for the designed antenna structure is shown in Fig. 2. L_P indicates the series inductance due to the rectangular patch of the antenna. The designed SRR plays a role for

(a)   (b)
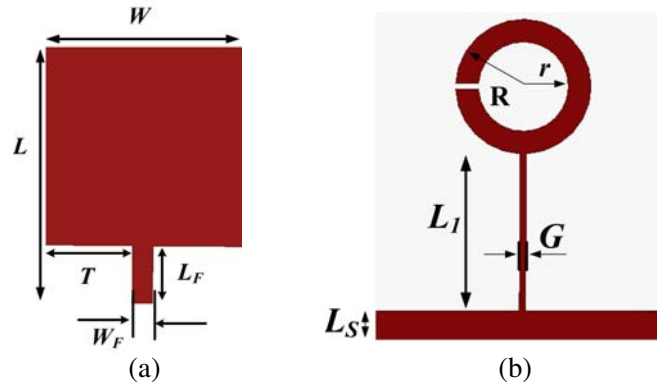
Figure 1. Dimension of proposed antenna (all the dimensions are in mm: $L = 30$, $L_1 = 10.5$, $L_F = 8$, $T = 9$, $R = 4.5$, $r = 3$, $G = 0.4$, $W = 20$, $W_S = 3$, $W_F = 2$). (a) top view, (b) bottom view.
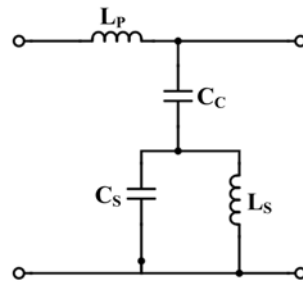
Figure 2. Equivalent circuit diagram for the designed wideband antenna.

shunt tank circuit of C_S and L_S, and C_C is the coupling capacitance between the rectangular patch and SRR. The equivalent circuit diagram for the designed antenna structure is similar to the equivalent circuit diagram for the epsilon negative transmission line. So dispersion relation for the designed antenna structure can be computed with the Bloch-Floquet theorem [7].

$$\beta d = \cos^{-1}(1 + (ZY)/2) \tag{1}$$

where Z, Y and d stand for the series impedance, shunt admittance and unit cell length of the designed antenna structure.

$$Z = (j\omega Lp) \text{ And } Y = (j\omega Cc)//(j\omega Cs + 1/j\omega Ls)$$

Since the designed antenna is configured with open-ended boundary condition, the ZOR frequency must be controlled by shunt parameters. In order to verify the above stated sentence, the values of Z and Y are substituted in Eq. (1).

$$\beta d = \cos^{-1}\left(1 + \frac{\left(\frac{\omega^2}{\omega_l^2}\right)\left(\frac{\omega^2}{\omega_m^2}\right) - \left(\frac{\omega^2}{\omega_l^2}\right)}{2\left(1 - \left(\frac{\omega^2}{\omega_n^2}\right)\right)}\right) \tag{2}$$

where $\omega_l = \frac{1}{\sqrt{LpCc}}$, $\omega_m = \frac{1}{\sqrt{LsCs}}$, $\omega_n = \frac{1}{\sqrt{Lp(Cs+Cc)}}$.

Further, the resonant mode can also be calculated by Eq. (3) [4].

$$\beta d = n\pi \tag{3}$$

where n indicates the number of modes.

In order to calculate ZOR mode, the value of n should be zero, which means no phase variation throughout the patch. From Eqs. (2) and (3) at ZOR mode, the ZOR frequency is calculated and presented in Eq. (4).

$$\omega_z = \omega_{ZOR} = \frac{1}{\sqrt{LsCs}} \tag{4}$$

It is clearly shown that the ZOR frequency can be controlled by varying the shunt parameters which is SRR in the designed antenna structure, hence open ended antenna configuration.

The input reflection coefficient at distinct values of R (Outer radius of SRR) is depicted in Fig. 3. It is observed that by varying R from 4.5 to 5.3 mm, the second resonance peak (at 3.41 GHz) starts
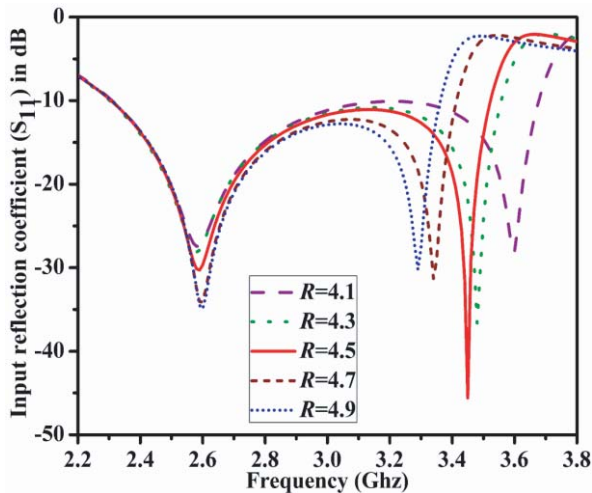
Figure 3. Variation in input reflection coefficient by varying the outer radius (R) of the split ring resonator.
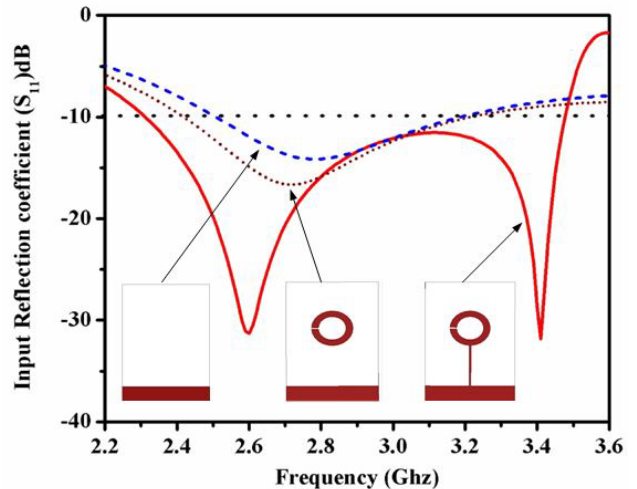
Figure 4. Input reflection coefficient of the designed antenna with and without split ring resonator and thin strip.

shifting towards lower frequencies. This shift is due to the increment of left-handed inductance (L_S) and right-handed capacitance (C_S), as in Eq. (4). In addition to above, this parametric analysis also suggests that the second resonance peak is the ZOR in Eq. (4).

Figure 4 shows input reflection coefficient of the designed antenna with and without split ring resonator and thin strip. It can be clearly observed that without SRR and thin strip the designed antenna offers a single resonance peak at the frequency of 2.78 GHz with the highest input reflection coefficient value of −14.15 dB. Without SRR and thin strip, the designed antenna structure offers −10 dB fractional bandwidth of 24.10% around the resonance frequency of 2.78 GHz. Further, the SRR along with thin strip is responsible for the origination of one new resonance peak. The dimensions of SRR are optimized, so that both the resonance peaks lie near each other. Due to this mode merging wide bandwidth is achieved. In addition to above, SRR and thin strip are also responsible for the improved impedance matching. After incorporating SRR and thin strip, the designed antenna offers an improved bandwidth of 40.13% at the center frequency of 2.89 GHz.

The electric field distribution plot on the top and bottom surfaces of the designed wideband antenna at both the resonance peaks of 2.61 GHz and 3.41 GHz is plotted and shown in Fig. 5. It is clearly seen that at the resonance peak of 2.61 GHz, the maximum electric field concentration is on the top patch of the antenna while at the resonance peak of 3.41 GHz, the maximum field concentration is on SRR. This indicates that the resonance peak at 2.61 GHz is originated from the patch of antenna while SRR is responsible for the origination of the second resonance peak of 3.41 GHz.

Figure 6 depicts the fabricated prototype of the designed wideband antenna structure used for the verification of simulated results. The graph of simulated and measured input reflection coefficients is depicted in Fig. 7. It is observed that the designed wideband antenna provides −10 dB simulated and measured fractional bandwidths of 40.13% and 40.55% with respect to the centre frequencies


(a) at 2.61 GHz

(b) at 3.41 GHz
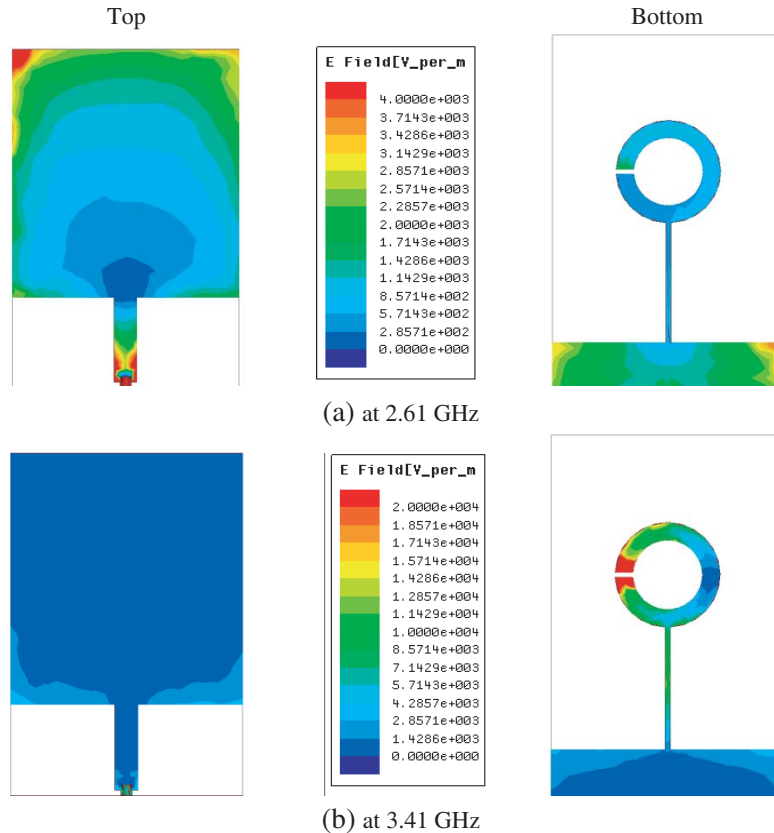
Figure 5. Electric field distribution plot on the top and bottom surface of the designed wideband antenna at (a) 2.61 GHz, (b) 3.41 GHz.

of 2.89 GHz and 2.88 GHz, respectively. Simulated and measured results show similar patterns and fractional bandwidths except a little deviation in the resonance frequencies. This small deviation in resonance frequency may be due to the non-uniformity of substrate and imperfection of connectors.

The simulated and measured radiation pattern plots, at both the resonance peaks, in both xz- and yz-planes, for the designed wideband antenna are presented in Fig. 8. It is observed that at both the resonance peaks, the proposed wideband antenna offers consistent omnidirectional radiation pattern. In addition to above, the designed wideband antenna offers better than -45 dB cross polarization in both planes at both the resonance peaks.

Figure 9 depicts the 3D gain plot at both the resonance peaks of the designed antenna structure. Fig. 10, shows simulated radiation efficiency along with simulated and measured average broadside gain plots for the designed wideband antenna. It is observed that in the entire -10 dB bandwidth, the designed antenna provides an average radiation efficiency of 96.2%. Additionally, it also offers average simulated and measured broadside gains of 1.92 dB and 1.75 dB, respectively. Table 1 shows the comparison of proposed work with previously published work. It can be clearly observed that in the presented table the SRR based antenna offers the highest bandwidth and radiation efficiency without much compromising with overall footprint area. In Table 1 except [2], the designed antenna offers the highest average gain throughout the working band.
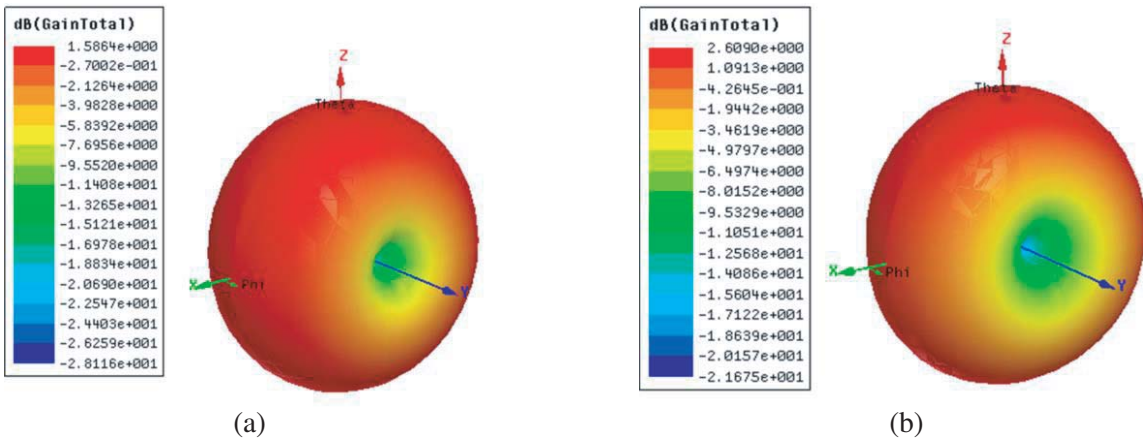

(a)   (b)
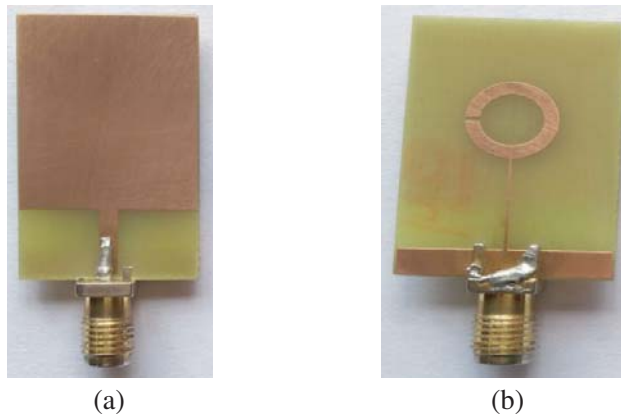
Figure 6. Fabricated prototype of the designed wideband antenna. (a) Top view. (b) Bottom view.
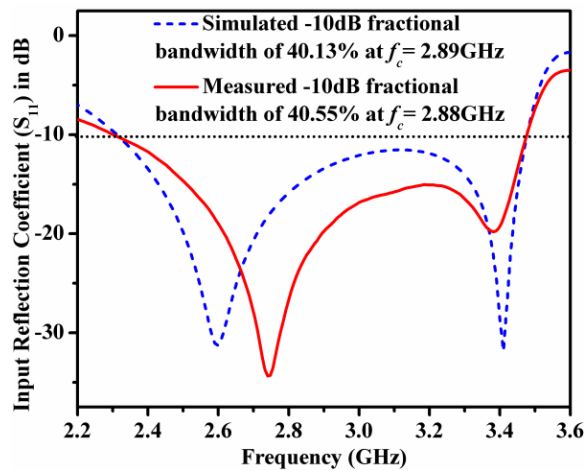
Figure 7. Simulated and measured input reflection coefficient response for the designed wideband antenna structure.
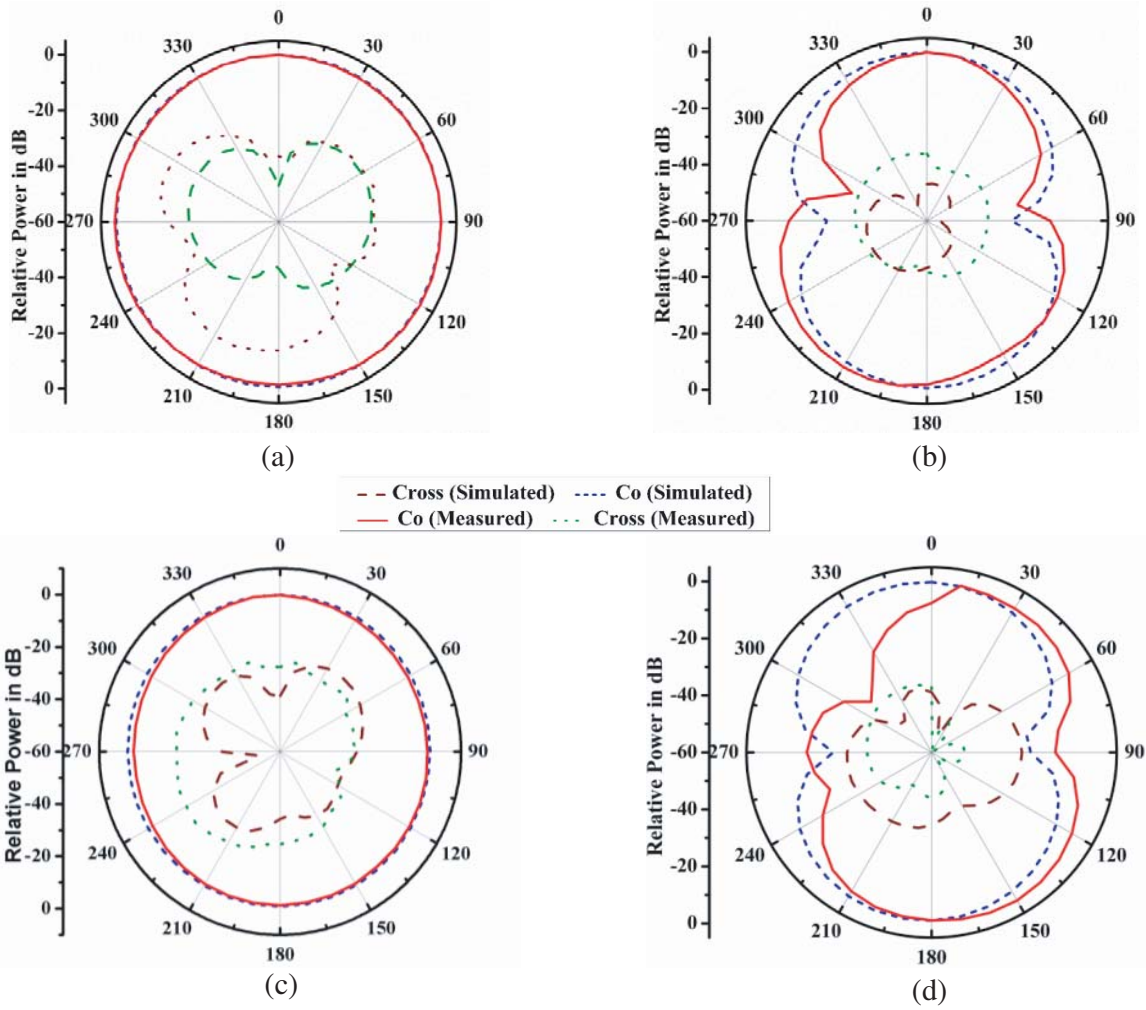
Figure 8. Simulated and measured radiation pattern plot. (a) at 2.61 GHz in xz-plane, (b) at 2.61 GHz in yz-plane, (c) at 3.41 GHz in xz-plane, (d) at 3.41 GHz in yz-plane.

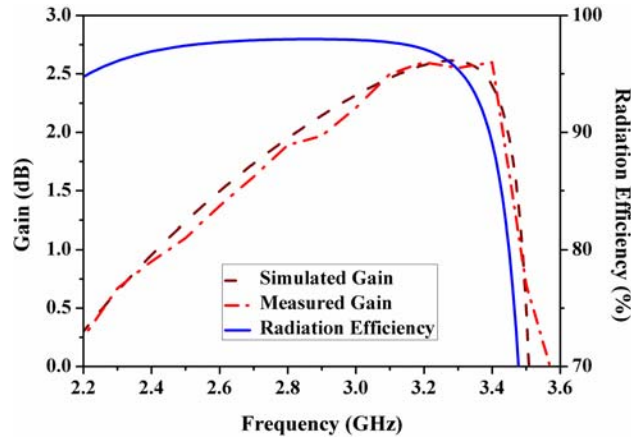**Figure 9.** Simulated 3D gain plot of the designed antenna at (a) 2.61 GHz, (b) 3.41 GHz.

Figure 10. Total gain (Broadside direction) and radiation efficiency of the designed antenna.

Table 1. Comparison of this work WITH previously reported work.

Parameter	This work	Previously reported work					
		[2]	[7]	[8]	[13]	[14]	[16]
Centre Frequency (GHz)	2.89	3.60	2.14	2.42	3.82	2.16	3.3
Antenna footprint (λ_0)	0.29×0.19	0.27×0.13	0.32×0.285	0.22×0.08	0.50×0.44	0.22×0.14	0.25×0.15
Inpedance Bandwidth (%)	40.55	23.64	5.3	1	6.8	15.1	3.1
Average Broadside Gain (dBi)	1.75	2.26	–	-0.53	–	1.62	0.79
Average Radiation Efficiency (%)	96.2	95.89	–	53	–	72	65.8

3. CONCLUSION

This article presents an SRR based compact wideband metamaterial inspired antenna for WiMAX /WLAN/Bluetooth /LTE applications. The designed antenna structure offers simulated and measured -10 dB fractional bandwidths of 40.13% and 40.55% around the center frequencies of 2.89 and 2.88 GHz, respectively. The overall electrical dimensions of the proposed antenna are $0.29\lambda_0 \times 0.19\lambda_0 \times 0.015\lambda_0$ where λ_0 represents the free space wavelength at the frequency of 2.89 GHz. The average simulated broadside gain and radiation efficiency throughout the entire -10 dB bandwidth are 1.92 dB and 96.2%, respectively. Further, the proposed antenna offers a consistent omnidirectional radiation pattern at both the resonance frequencies.

ACKNOWLEDGMENT

REFERENCES

1. Caloz, C. and T. Itoh, *Electromagnetic Metamaterials: Transmission Line Approach and Microwave Applications*, Wiley, Hoboken, NJ, 2005.

2. Mishra, N. and R. K. Chaudhary, "A miniaturized ZOR antenna with enhanced bandwidth for WiMAX applications," *Microwave and Optical Technology Letters*, Vol. 58, 71–75, 2016.

3. Ji, J. K., G. H. Kim, and W. M. Seong, "Bandwidth enhancement of metamaterial antennas based on composite right/left-handed transmission line," *IEEE Antennas Wireless Propagation Letters*, Vol. 9, 36–39, 2010.

4. Jang, T., J. Choi, and S. Lim, "Compact coplanar waveguide (CPW)-fed zeroth-order resonant antennas with extended bandwidth and high efficiency on via-less single layer," *IEEE Trans. Antennas Propagation*, Vol. 59, 363–37, 2011.

5. Lee, C. J., K. M. K. H. Leong, and T. Itoh, "Compact dual-band antenna using an anisotropic metamaterial," *36th European Microwave Conference*, 1044–1047, Manchester, UK, 2006.

6. Lai, A., K. M. K. H. Leong, and T. Itoh, "Infinite wavelength resonant antennas with monopolar radiation pattern based on periodic structures," *IEEE Trans. Antennas Propagation*, Vol. 55, 868–876, 2007.

7. Gupta, A., S. K. Sharma, and R. K. Chaudhary, "A compact dual-mode metamaterial-inspired antenna using rectangular type CSRR," *Progress In Electromagnetics Research C*, Vol. 9, 36–39, 2015.

8. Liu, C. C., P. L. Chi, and Y. D. Lin, "Compact zeroth-order resonant antenna based on dual-arm spiral configuration," *IEEE Antennas and Wireless Propagation Letters*, Vol. 11, 318–321, 2012.

9. Kim, J., C. S. Cho, and J. W. Lee, "CPW bandstop filter using slot type SRRs," *Electronics Lett.*, Vol. 41, 2005.

10. Fouad, M. A. and M. A. Abdalla, "New π-T generalised metamaterial negative refractive index transmission line for a compact coplanar waveguide triple band pass filter applications," *IET Microwave. Antennas Propagations*, Vol. 8, 1097–1104, 2014.

11. Mishra, N., D. K. Choudhary, R. Chowdhury, K. Kumari, and R. K. Chaudhary, "An investigation on compact ultra-thin triple band polarization independent metamaterial absorber for microwave frequency applications," *IEEE Access*, Vol. 5, 437–4376, 2017.

12. Kumari, K., N. Mishra, and R. K. Chaudhary, "An ultra-thin compact polarization insensitive dual band absorber based on metamaterial for X-band applications," *Microwave and Optical Technology Letters*, Vol. 59, 2664–2669, 2017.

13. Ha, J., K. Kwon, Y. Lee, and J. Choi, "Hybrid mode wideband patch antenna loaded with a planar metamaterial unit cell," *IEEE Trans. Antennas Propagation*, Vol. 60, 1143–1147, 2012.

14. Chi, P.-L. and Y.-S. Shih, "Compact and bandwidth-enhanced zeroth order resonant antenna," *IEEE Antennas Wireless Propagation Letters*, Vol. 14, 285–288, 2015.

15. Sharma, S. K. and R. K. Chaudhary, "A compact zeroth-order resonating wideband antenna with dual-band characteristics," *IEEE Antennas and Wireless Propagation Letters*, Vol. 14, 1670–1672, 2015.

16. Zhu, J. and G. V. Eleftheriades, "A compact transmission line metamaterial antenna with extended bandwidth," *IEEE Antennas and Wireless Propagation Letters*, Vol. 8, 295–298, 2009.

17. Kenari, M. A., M. N. Moghadasi, B. S. Virdee, A. Andújar, and J. Anguera, "Compact antenna based on a composite right/left-handed transmission line," *Microwave and Optical Technology Letters*, Vol. 57, 1785–1788, 2015.

18. Kenari, M. A., B. S. Virdee, A. Ali, and E. Limiti, "A novel monofilar-Archimedean metamaterial inspired leaky-wave antenna for scanning application for passive radar systems," *Microwave and Optical Technology Letters*, Vol. 60, 2055–2060, 2018.

19. Kenari, M. A., M. N. Moghadasi, R. A. Sadeghzadeh, B. S. Virdee, and E. Limiti, "Traveling-wave antenna based on metamaterial transmission line structure for use in multiple wireless communication applications," *AEU-International Journal of Electronics and Communications*, Vol. 70, 1645–1650, 2016.